

Modelling charge transport in perovskite solar cells: Potential-based and limiting ion vacancy depletion

Dilara Abdel, Petr Vágner, Jürgen Fuhrmann, Patricio Farrell

submitted: October 20, 2020

Weierstrass Institute
Mohrenstr. 39
10117 Berlin
Germany
E-Mail: dilara.abdel@wias-berlin.de
petr.vagner@wias-berlin.de
juergen.fuhrmann@wias-berlin.de
patricio.farrell@wias-berlin.de

No. 2780
Berlin 2020



2020 Mathematics Subject Classification. 35Q81, 35K57, 65N08.

Key words and phrases. Finite volume methods, perovskite solar cells, semiconductor device modelling, drift-diffusion equations, Scharfetter-Gummel methods.

This work was partially supported by the German Research Foundation, DFG project no. FU 316/14-1 as well as the Leibniz competition.

Edited by
Weierstraß-Institut für Angewandte Analysis und Stochastik (WIAS)
Leibniz-Institut im Forschungsverbund Berlin e. V.
Mohrenstraße 39
10117 Berlin
Germany

Fax: +49 30 20372-303
E-Mail: preprint@wias-berlin.de
World Wide Web: <http://www.wias-berlin.de/>

Modelling charge transport in perovskite solar cells: Potential-based and limiting ion vacancy depletion

Dilara Abdel, Petr Vágner, Jürgen Fuhrmann, Patricio Farrell

Abstract

From Maxwell-Stefan diffusion and general electrostatics, we derive a drift-diffusion model for charge transport in perovskite solar cells (PSCs) where any ion in the perovskite layer may flexibly be chosen to be mobile or immobile. Unlike other models in the literature, our model is based on quasi Fermi potentials instead of densities. This allows to easily include nonlinear diffusion (based on for example Fermi-Dirac, Gauss-Fermi or Blakemore statistics) as well as limit the ion vacancy depletion (via the Fermi-Dirac integral of order -1). The latter will be motivated by a grand-canonical formalism of ideal lattice gas. Furthermore, our model allows to use different statistics for different species. We discuss the thermodynamic equilibrium, electroneutrality as well as generation/recombination. Finally, we present numerical finite volume simulations to underline the importance of limiting ion vacancy depletion.

1 Introduction

In recent years, perovskite solar cells (PSCs) have become one of the fastest growing technology within photovoltaics [1, 2]. Typically, in a PSC a perovskite layer is sandwiched between an electron transport layer (ETL) and a hole transport layer (HTL), see Figure 1.1a. One of the most common device architectures is a planar cell, where light enters through the ETL. If light enters through the HTL, the architecture is called inverted.

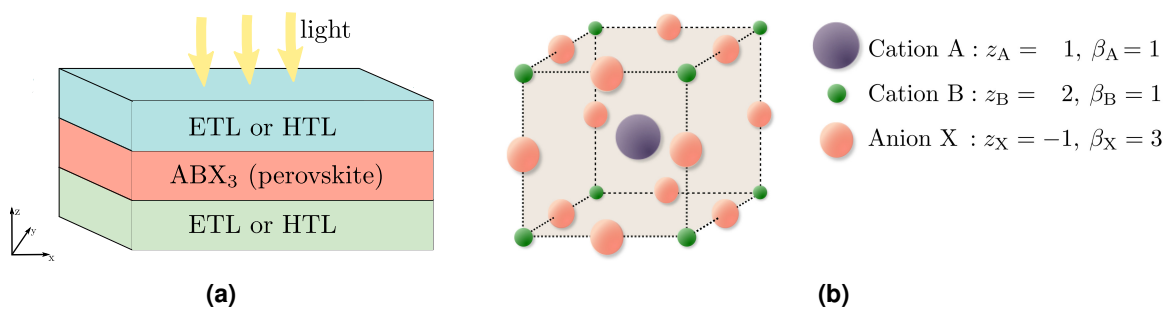


Figure 1.1: (a) A perovskite solar cell architecture. For simplicity other layers have been neglected to focus on the charge transport within the perovskite. Typically, TiO_2 , PCBM, ZnO are chosen as ETL material, whereas spiro-OMeTAD and PEDOT:PSS are common materials for the hole transport layer. (b) A perovskite unit cell with corresponding charge numbers z_α and lattice weights β_α , see Sections 2.3 and 2.4 for more details.

Two advantages of PSCs stand out: On the one hand, certain architectures have significantly lower production costs than conventional solar cells. On the other hand, in 2020 silicon-perovskite tandem cells have become more efficient than classical single junction silicon solar cells. A record efficiency of

29.15% has been demonstrated [1, 3]. Further efficiency gains are likely. However, the commercialization of PSCs is still in its early stages and several challenges need to be overcome: Commercially viable PSCs degrade significantly faster. Also some PSCs rely on environmentally unfriendly materials such as lead (Pb), yielding toxic chemical compounds (PbI_2).

For this reason it is paramount to understand the charge transport in perovskites better via improved modelling and simulation. A major difference to charge transport models for classical or organic semiconductors is that ion migration within the perovskite plays a fundamental role. Adequate models which include all relevant physical effects are also crucial for numerical simulations to better predict the behavior of such complex physical devices.

Already in the 80ies, the diffusion of ionic vacancies was studied [4]. However, only in 2014 ion migration in perovskite devices became of practical interest when experiments seemed to indicate that the mobility of ionic defects is one possible reason for current-voltage hysteresis in perovskite solar cells [5]. In 2015, Eames et al. presented a density functional theory (DFT) model [6]. Due to DFT's exceedingly high computational costs as well its inability to produce I-V characteristics which can be compared to experiments, various drift-diffusion models were formulated – first without, e.g. [7], and later with ion migration. Also in 2015, van Reenen et al. formulated a drift-diffusion model incorporating ionic transport [8]. Shortly after, Calado et al. [9], Courtier et al. [10, 11], and Neukom et al. [12] presented extended drift-diffusion systems to model charge transport in perovskite solar cells.

All of these models above are based on densities and linear diffusion (the Boltzmann approximation). Densities depend on the continuous quasi Fermi potentials but are discontinuous themselves across heterojunctions. While densities have an intuitive interpretation, they lack a certain flexibility from a modelling and computational point of view. For this reason, we present a model which is based on quasi Fermi potentials. Using quasi Fermi potentials instead of densities as set of unknowns has several practical advantages: First, they are on the same order of magnitude as the electrostatic potential and do not vary over more than twenty orders of magnitude like densities may do. This is advantageous from a numerical point of view. Second, unlike densities quasi Fermi potentials are continuous across heterojunctions. Yet, no additional discontinuity-preserving internal boundary conditions for the densities are needed. Third, potentials are easier to interpret physically as well as mathematically e.g. as gradient flows [13, 14, 15].

But perhaps most importantly a potential-based model allows to easily include two important features which thus far seem to have been neglected almost entirely in the perovskite literature: In three-dimensional (3D) bulk semiconductors with parabolic bands the statistical relationship which links densities to quasi-Fermi potentials is given by the Fermi-Dirac integral of order one-half [16]. This leads to nonlinear diffusion in the charge transport equations. This nonlinearity cannot be neglected in highly doped regions, at low temperatures or in certain organic materials [17]. So far it seems only Fell et al. [18] and Tessler et al. [19] have used statistical relationships which do not rely on the simpler Boltzmann approximation for the charge carrier densities of electrons and holes within the perovskite literature.

Moreover, neither of the previously mentioned models limit the depletion of ion vacancies. Physically one cannot extract ions below a certain threshold without destroying the perovskite's crystal structure. We will enforce this threshold by employing the Fermi-Dirac integral of order -1 [20] which we will properly derive from a grand canonical formalism of ideal lattice gas. Recently this feature has been hardcoded into a FEM based drift-diffusion code [21, 22] but to the best of our knowledge all standard perovskite drift-diffusion models seem to not limit ion vacancy depletion.

The remainder of this paper is organized as follows: In Section 2, we derive our general drift-diffusion model for charge transport in perovskite solar cells from Maxwell-Stefan diffusion and electrostatics. Ionic migration is assumed due to Schottky defects. The model allows all three ionic species to be

mobile though in practice this does not seem to be necessary [12]. We also discuss useful aspects such as thermodynamic equilibrium, local electroneutrality as well as photogeneration and recombination. We motivate our specific choice for how to limit the ion vacancies and finish this section by formulating a simplified model for just one mobile ionic species. Another useful additional feature of our model is that the governing statistics may be chosen for each charge carrier individually. In Section 3, we briefly present numerical simulations that emphasize the importance of limiting ion vacancy depletion. From our simulation it becomes apparent that not properly limiting the ions will overestimate their influence on the electrons and holes. While others have used either a finite-difference [11, 18], a finite-element discretization [9, 11], or commercial software packages [12, 23, 24, 25, 26], we use a physics preserving finite volume discretization [17, 27]. Finally, we conclude in Section 4. In the appendices, we describe our numerical method and link our notation to the existing literature.

2 Drift-diffusion model for charge transport in perovskite solar cells

2.1 Electrostatics and mass balances

We develop our transport model from a general system of nonlinear partial differential equations, consisting of the self-consistent Poisson equation for the electrostatic potential as well as balance equations for the particle densities. To this end, we consider a mixture of charged species α with particle densities n_α , and the electrostatic potential ψ which is linked to the electrical field via $\mathbf{E} = -\nabla\psi$ in an isothermal electrostatic setting. The general system reads

$$-\nabla \cdot (\varepsilon_s \nabla \psi) = q \sum_{\alpha \in \mathbb{M}} z_\alpha n_\alpha, \quad (2.1.1a)$$

$$\partial_t n_\alpha + \nabla \cdot \mathbf{J}_\alpha = r_\alpha, \quad \alpha \in \mathbb{M}, \quad (2.1.1b)$$

where q is the positive elementary charge and $z_\alpha \in \mathbb{Z}$ denotes the charge number of species α . The species are labeled by a finite index set \mathbb{M} . With $\varepsilon_s = \varepsilon_0 \varepsilon_r$ we refer to the dielectric permittivity, where ε_0 is the vacuum dielectric constant and ε_r the relative permittivity of the material. The particle fluxes are given by \mathbf{J}_α and the density production/reduction rates of species α are denoted by r_α . We point out that system (2.1.1) is formulated in terms of densities. Eventually we will rewrite the system in terms of quasi Fermi potentials φ_α . In the next sections, we introduce Maxwell-Stefan diffusion and develop the electrostatics for our specific setup.

2.2 Maxwell-Stefan diffusion and electrostatic drift

Once partial momenta of the species are relaxed and the system is isothermal, the friction between the species can be modelled with Maxwell-Stefan diffusion [28, 29] and electrostatic drift via

$$n_\alpha (\nabla \Phi_\alpha + z_\alpha q \nabla \psi) = \sum_{\beta \in \mathbb{M}, \beta \neq \alpha} \zeta_{\alpha\beta} \left(\frac{\mathbf{J}_\beta}{n_\beta} - \frac{\mathbf{J}_\alpha}{n_\alpha} \right), \quad \alpha \in \mathbb{M}, \quad (2.2.1)$$

where Φ_α denotes the chemical potential (per particle) of species α (see [30, (18.2.4)]), and $\zeta_{\alpha\beta} = \zeta_{\beta\alpha}$ the symmetric binary friction coefficient between species α and β . The quantities $\mathbf{J}_\alpha/n_\alpha$ correspond to the velocities of species α . Let us assume that one of the species within the mixture represents the

lattice with index L and, moreover, that the friction is solely observed as an interaction between the lattice and the other species,

$$\zeta_{\alpha\beta} = 0 \quad \text{and} \quad \zeta_{\alpha L} \geq 0, \quad \alpha, \beta \in \mathbb{M} \setminus \{L\}.$$

In order to avoid that the lattice species n_L appears in the mass balances (2.1.1b), we describe the transport of the species $\alpha \in \mathbb{M} \setminus \{L\}$ from the viewpoint of the crystalline lattice. In other words, we set $\mathbf{J}_L = 0$ and assume that the lattice species is not produced, $r_L = 0$. This implies by (2.1.1b) that $\partial_t n_L = 0$. Finally, we assume that the friction does not cause a deformation of the lattice.

Moreover, we distinguish between mobile and stationary (immobile) species and refer to the latter with the index set $\mathbb{S} \subset \mathbb{M}$. Hence, we model the different particle fluxes by

$$\mathbf{J}_\alpha = -\frac{n_\alpha}{\zeta_{\alpha L}} n_\alpha (\nabla \Phi_\alpha + z_\alpha q \nabla \psi), \quad \alpha \in \mathbb{M} \setminus (\mathbb{S} \cup \{L\}), \quad (2.2.2)$$

$$\mathbf{J}_\alpha = 0, \quad \alpha \in \mathbb{S} \cup \{L\} \quad (2.2.3)$$

and assume zero production of immobile species, i.e.

$$r_\alpha = 0, \quad \text{for } \alpha \in \mathbb{S} \cup \{L\}.$$

2.2.1 The quasi Fermi vs. electrochemical potential

In analogy to semiconductor theory, we use the following relation between the chemical Φ_α , the electrostatic ψ and the quasi Fermi potential φ_α ,

$$\varphi_\alpha = \frac{1}{z_\alpha q} \Phi_\alpha + \psi, \quad (2.2.4)$$

see also [30]. Using this definition, we can highlight the fact that the gradient of the quasi Fermi potentials are the driving forces of the current particle densities (2.2.2)

$$\mathbf{J}_\alpha = -z_\alpha q \frac{n_\alpha}{\zeta_{\alpha L}} n_\alpha \nabla \varphi_\alpha, \quad \alpha \in \mathbb{M} \setminus (\mathbb{S} \cup \{L\}).$$

2.2.2 Continuity equations and electric currents

The charge density carried by species α is given by $z_\alpha q n_\alpha$. The electric current \mathbf{j}_α observed due to the transport of species α is related to the particle flux \mathbf{J}_α by

$$\underbrace{\mathbf{j}_\alpha}_{\text{electric current}} = z_\alpha q \underbrace{\mathbf{J}_\alpha}_{\text{particle current}}, \quad \alpha \in \mathbb{M} \setminus (\mathbb{S} \cup \{L\}). \quad (2.2.5)$$

We define the friction coefficients as

$$\zeta_{\alpha L} = q \frac{n_\alpha}{\mu_\alpha}, \quad (2.2.6)$$

with phenomenological units $\text{kg}/(\text{m}^3\text{s})$, where μ_α describes the mobility of species α . In other words, the electric current becomes

$$\mathbf{j}_\alpha = -(z_\alpha q)^2 \frac{n_\alpha}{\zeta_{\alpha L}} n_\alpha \nabla \varphi_\alpha = -(z_\alpha)^2 q \mu_\alpha n_\alpha \nabla \varphi_\alpha, \quad \alpha \in \mathbb{M} \setminus (\mathbb{S} \cup \{L\}). \quad (2.2.7)$$

For such an electric flux the general drift-diffusion equation (2.1.1b) now finally reads

$$z_\alpha q \partial_t n_\alpha + \nabla \cdot \mathbf{j}_\alpha = z_\alpha q r_\alpha, \quad \alpha \in \mathbb{M} \setminus (\mathbb{S} \cup \{L\}). \quad (2.2.8)$$

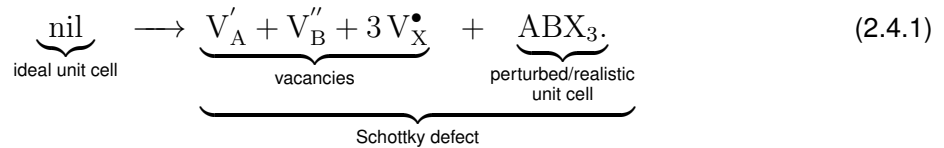
We emphasize that the carrier densities n_α depend on the quasi Fermi potentials φ_α and the electrostatic potential ψ , i.e. $n_\alpha = n_\alpha(\psi, \varphi_\alpha)$. We will address this in Section 2.6. With this dependence (2.2.8) can be written exclusively in terms of potentials.

2.3 Perovskite structure

Perovskites have a general crystalline structure of the form ABX_3 , where A and B denote positively charged cations and X a negatively charged anion. A perovskite unit cell is depicted in Figure 1.1b. Since the ABX_3 structure is general, several different choices for the anions and cations are possible. Typically, the cation A is chosen to be an organic ion such as methylammonium (MA) or formamidinium (FA), whereas the other cation is a metal, frequently $B = \text{Pb}$ or $B = \text{Sn}$, and lastly, we have a halide anion X, which is commonly chosen to be either I, Br, or Cl. The most commonly used combination is methylammonium ($A = \text{CH}_3\text{NH}_3 = \text{MA}$), lead ($B = \text{Pb}$), and iodine ($X = \text{I}$), resulting into methylammonium lead (tri-)iodide $ABX_3 = (\text{CH}_3\text{NH}_3)(\text{Pb})(\text{I}_3)$. These anions and cations interact to some extent with electrons and holes as we will discuss in the following section.

2.4 Schottky defects in perovskites

Ionic movement in perovskites is due to Schottky defects [6] which can be expressed via the Kröger-Vink notation, namely



Here, nil denotes the ideal perovskite crystalline lattice. The ions dislocate from their ideal positions, forming vacancies V_α in the ideal lattice. The superscript ' denotes a negative charge and the superscript • denotes a positive charge. We assume that each Schottky defect creates the oppositely charged vacancies V'_A , V''_B and $3V^\bullet_X$ and, furthermore, that each vacancy V_α can be occupied by an ionic species $\alpha \in \mathbb{I}$, where $\mathbb{I} = \{A, B, X\}$ is the index set of all ionic species.

Hence, assuming imperfections of the unit cell, allows (at least in theory) both cation as well as the anion species to move. Thus, for the ion and vacancy densities we have the following relationship:

$$\underbrace{n_\alpha}_{\text{reality}} = \underbrace{\bar{n}_\alpha}_{\text{ideal}} - \underbrace{n_{V_\alpha}}_{\text{vacancy}}, \quad \alpha \in \mathbb{I}. \quad (2.4.2)$$

Additionally, the ideal ion density \bar{n}_α can be linked to the ideal lattice density \bar{n}_L via

$$\beta_\alpha \bar{n}_L = \bar{n}_\alpha, \quad \alpha \in \mathbb{I}, \quad (2.4.3)$$

where β_α denotes a dimensionless lattice weight. The parameter β_α can be determined by counting the number of ionic species in each ideal unit cell, respecting shared faces and edges with neighboring unit cells, see Figure 1.1b. Since we assume no defect in the ideal lattice, $\bar{n}_L = n_L$ holds. The charge

numbers z_α with the corresponding lattice weights β_α are given in Table 2.1. For the ion vacancies we have $z_{V_\alpha} = -z_\alpha$ and $\beta_{V_\alpha} = \beta_\alpha$.

	A	B	X	n	p	N_A	N_D	L
charge number z_α	1	2	-1	-1	1	-1	1	0
lattice weight β_α	1	$\frac{8}{8} = 1$	$\frac{12}{4} = 3$	-	-	-	-	-

Table 2.1: Charge numbers z_α and lattice weights β_α .

The relationship in (2.4.3) becomes apparent, when considering that

$$\bar{n}_L = \frac{\#(\text{unit cells})}{\text{volume of material}} = \frac{1}{\text{volume of unit cell}},$$

and identifying β_α as the *ideal weighted number of ion α* in the unit cell.

2.5 Poisson equation for intrinsic perovskites and doped semiconductors

From this section on, we more focus on the specific index set $\mathbb{M} = \mathbb{I} \cup \{n, p\} \cup \{L\} \cup \mathbb{S}$ where the stationary species are given by $\mathbb{S} = \{N_A, N_D\}$ and the ionic species by $\mathbb{I} = \{A, B, X\}$. Here n and p refer to the electron and hole indices. For simplicity, we introduce the abbreviation $N_A = n_{N_A}$ and $N_D = n_{N_D}$, which refer to the density of singly ionized donor and acceptor atoms, respectively. The corresponding charge numbers can be found in Table 2.1. Next, we adapt the right-hand side of the general Poisson equation (2.1.1a) to several more specific cases. These choices become evident in Section 2.6 where we formulate the final drift-diffusion model.

Case 1 Doped non-perovskite semiconductor material:

$$-\nabla \cdot (\varepsilon_s \nabla \psi) = q \left((n_p - N_A) - (n_n - N_D) \right). \quad (2.5.1)$$

Case 2 Intrinsic perovskite material (three mobile ions):

$$q \sum_{\alpha \in \mathbb{M}} z_\alpha n_\alpha \stackrel{(2.4.2)}{=} q (n_p - n_n) + q \sum_{\alpha \in \mathbb{I}} z_\alpha (\bar{n}_\alpha - n_{V_\alpha}).$$

From (2.4.3) we know that we can relate the ideal ionic density \bar{n}_α , $\alpha \in \mathbb{I}$, to the lattice density \bar{n}_L . Since the perovskite unit cell is electroneutral, we have $q \bar{n}_L \sum_{\alpha \in \mathbb{I}} z_\alpha \beta_\alpha = 0$, see also Table 2.1. Hence,

$$-\nabla \cdot (\varepsilon_s \nabla \psi) = q (n_p - n_n) - q \sum_{\alpha \in \mathbb{I}} z_\alpha n_{V_\alpha}. \quad (2.5.2)$$

Case 3 Intrinsic perovskite material (one mobile X ion):

As reported in [6], for $ABX_3 = \text{CH}_3\text{NH}_3\text{PbI}_3$, the hopping of $X = \text{I}^-$ seems to have the lowest energy barrier and according to experiments [9], it is reasonable to assume that both cations A and B move on significantly larger time scales. Therefore, in some applications it is convenient to consider a simplified model, where only the anion species X is assumed to be mobile, as done in [9, 10].

Let us assume local electroneutrality, that is the left-hand side of (2.5.2) vanishes. In this case, we assume a temperature dependent density of the Schottky defects

$$N_{\text{SD}} = N_{\text{SD}}(T) = \frac{\#(\text{defective cells})}{\text{volume of material}},$$

which is linked to the vacancy densities n_{V_α} via

$$n_{V_\alpha} = \beta_\alpha N_{\text{SD}} \quad \text{if locally electroneutral.}$$

Further, we can relate the Schottky defect density N_{SD} to the lattice density \bar{n}_L with a parameter $\kappa_{\text{SD}} \in [0, 1]$ by

$$\kappa_{\text{SD}} \bar{n}_L = N_{\text{SD}}.$$

Then, for the immobile vacancies the following expression can be inserted in (2.5.2)

$$n_{V_\alpha} = \beta_\alpha \kappa_{\text{SD}} \bar{n}_L, \quad \alpha \in \{A, B\}.$$

We define a constant and uniform density of immobile cation vacancies (see also [11]): $C_0 := (z_{V_A} \beta_A + z_{V_B} \beta_B) \kappa_{\text{SD}} \bar{n}_L$. Then the Poisson equation becomes

$$-\nabla \cdot (\varepsilon_s \nabla \psi) = q (n_p - n_n + n_{V_X} - C_0). \quad (2.5.3)$$

In the literature [9, 11] it is suggested to choose C_0 equal to the average anion vacancy density.

Case 4 Intrinsic perovskite material (mobile A and X ion):

There are modeling approaches known [8, 12, 18, 21], where mobile A and X ions are assumed. In analogy to case 3, the Poisson equation in (2.1.1a) can be simplified. We assume a constant and uniform density of immobile B vacancies $C_0 := z_B \beta_B \kappa_{\text{SD}} \bar{n}_L$ and obtain

$$-\nabla \cdot (\varepsilon_s \nabla \psi) = q (n_p - n_n + n_{V_X} - n_{V_A} - C_0). \quad (2.5.4)$$

2.6 Final drift-diffusion model

In the following, we consider a bounded spatial domain $\Omega \subseteq \mathbb{R}^d$, $d \in \{1, 2, 3\}$, such that

$$\Omega = \Omega_{\text{HTL}} \cup \Omega_{\text{intr}} \cup \Omega_{\text{ETL}},$$

where $\Omega_{\text{HTL}}, \Omega_{\text{intr}}, \Omega_{\text{ETL}} \subseteq \Omega$ are pairwise disjoint, open subsets. Here, Ω_{intr} refers to the intrinsic perovskite region and $\Omega_{\text{HTL}}, \Omega_{\text{ETL}}$ to the doped non-perovskite semiconductor regions, respectively. The aim now is to carefully establish a potential-based drift-diffusion model for the description of charge transport in perovskite solar cells which takes into account that there must be a natural limit for the amount of ion vacancies, whose index set is given by $\mathbb{I}_V = \{V_A, V_B, V_X\}$ in the following for the sake of readability. Since we consider vacancies instead of ions, see (2.4.2), certain adjustments with respect to the index set in (2.1.1) are necessary. Let $t \in [0, t_F]$, then the model for charge transport in PSCs consists of two different parts:

Drift-diffusion model for PSCs

- 1 In the perovskite for $\mathbf{x} \in \Omega_{\text{intr}}$:
 - Poisson equation (2.5.2) for $\alpha \in \{n, p\} \cup \mathbb{I}$,
 - drift-diffusion equation (2.2.8) for $\alpha \in \{n, p\} \cup \mathbb{I}_V$ with $r_n = r_p = G(\mathbf{x}) - R(n, p)$ and $r_\alpha = 0$ for $\alpha \in \mathbb{I}_V$.
- 2 In transport layers for $\mathbf{x} \in \Omega_{\text{HTL}} \cup \Omega_{\text{ETL}}$:
 - Poisson equation (2.5.1) for $\alpha \in \{n, p\} \cup \{N_D, N_A\}$,
 - drift-diffusion equation (2.2.8) for $\alpha \in \{n, p\}$ with $r_n = r_p = G(\mathbf{x}) - R(n, p)$.

In summary, the model is given by six coupled equations in the intrinsic layer and three coupled equations in the transport layers supplemented with initial and boundary conditions which will be given in Section 2.10. Furthermore, G denotes the photogeneration and R the recombination rate. Both rates will be defined more carefully in Section 2.11.

As mentioned earlier, it is possible to link the densities n_α with their quasi Fermi potentials φ_α via some statistical relation [16], namely

$$n_\alpha = N_\alpha \mathcal{F}_\alpha \left(\eta_\alpha(\psi, \varphi_\alpha) \right), \quad \eta_\alpha = z_\alpha \frac{q(\varphi_\alpha - \psi) + E_\alpha}{k_B T}, \quad (2.6.1)$$

where \mathcal{F}_α describes the carrier statistics, N_α denotes an effective density and E_α an energy. We assume that \mathcal{F}_α is continuously differentiable and monotonously increasing. Several different physically relevant choices for \mathcal{F}_α will be discussed in Section 2.7. To see the connection to the literature, we express the electric fluxes (2.2.7) mathematically equivalent in terms of densities. For this, we introduce the generalized Einstein relation

$$D_\alpha = \mu_\alpha U_T g_\alpha(\eta_\alpha), \quad (2.6.2)$$

where $U_T = k_B T / q$ is the thermal voltage, k_B denotes the Boltzmann constant, T the constant absolute temperature, and g the *nonlinear diffusion enhancement* [31] given by

$$g_\alpha(\eta_\alpha) = \frac{\mathcal{F}_\alpha(\eta_\alpha)}{\mathcal{F}_\alpha'(\eta_\alpha)}. \quad (2.6.3)$$

Mathematically, the diffusion enhancement can be seen as nonlinear, potential-dependent diffusion. With the help of the generalized Einstein relation (2.6.2) it is now possible to derive the electric currents in drift-diffusion form

$$\mathbf{j}_\alpha = -q \left(z_\alpha D_\alpha \nabla n_\alpha + z_\alpha^2 \mu_\alpha n_\alpha \nabla \psi \right), \quad (2.6.4)$$

where the diffusion may be nonlinear. We stress that the diffusion enhancement g_α in (2.6.3) can be equivalently reformulated in terms of densities

$$g_\alpha \left(\frac{n_\alpha}{N_\alpha} \right) = \frac{n_\alpha}{N_\alpha} (\mathcal{F}_\alpha^{-1})' \left(\frac{n_\alpha}{N_\alpha} \right). \quad (2.6.5)$$

For different statistics functions \mathcal{F}_α the expression for the diffusion enhancement g_α in (2.6.5) is portrayed in Figure 2.1b.

2.7 Statistics function

In the following, we specify the functions \mathcal{F}_α in (2.6.1). Three common choices are conceivable:

$$\mathcal{F}_\alpha(\eta) = \exp(\eta), \quad (\text{Boltzmann}) \quad (2.7.1)$$

$$\mathcal{F}_\alpha(\eta) = F_{B,\gamma}(\eta) := \frac{1}{\exp(-\eta) + \gamma}, \quad (\text{Blakemore}) \quad (2.7.2)$$

$$\mathcal{F}_\alpha(\eta) = F_j(\eta) := \frac{1}{\Gamma(j+1)} \int_0^\infty \frac{\xi^j}{\exp(\xi - \eta) + 1} d\xi, \quad j > -1. \quad (\text{Fermi-Dirac}) \quad (2.7.3)$$

The Fermi-Dirac integral of order one-half [16], denoted by $F_{1/2}$, with $\Gamma(1/2 + 1) = \sqrt{\pi}/2$, is fundamental in the simulation of inorganic, classical three-dimensional (3D) semiconductors [17, 32]. The Gauss-Fermi integral [33] is the statistics of choice in the context of organic semiconductors. These integrals can be approximated by Blakemore ($\gamma = 0.27$) [34] and by Boltzmann statistics in the low density limit.

Remark 2.7.1. Via the relation $F'_j(\eta) = F_{j-1}(\eta)$, the Fermi-Dirac statistics (2.7.3) can be defined for negative integers j as well [20]. In particular, for order -1 , we have

$$F_{-1}(\eta) = \frac{1}{\exp(-\eta) + 1}.$$

We observe that $F_{-1} = F_{B,1}$. This type of statistics corresponds physically to a mean-field ideal lattice gas, see [35, Eqn. 3.5.1].

Figure 2.1 shows different \mathcal{F}_α along with their corresponding diffusion enhancements. Statistics functions deviating from the Boltzmann approximation lead to nonlinear diffusion which grows for larger densities/potentials as can be seen from (2.6.2) and (2.6.3) or visually in Figure 2.1b. This complicates the numerical solution of the model.

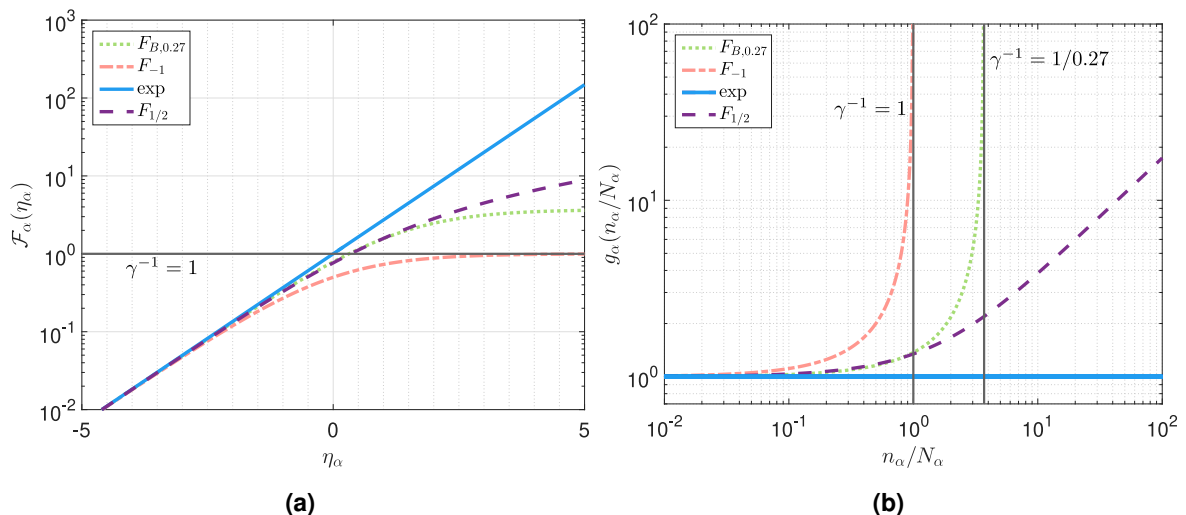


Figure 2.1: (a) Semi-logarithmic plot of the introduced distribution functions \mathcal{F}_α for $-5 \leq \eta_\alpha \leq 5$. (b) Logarithmic plot of the diffusion enhancement g_α for the statistics functions in (a), where we used (2.6.5). It can be observed that the charge carrier density can be limited by the Blakemore function ($\gamma = 1$) which agrees with the Fermi-Dirac integral of order -1 .

2.7.1 Charge carrier densities

We assume that the electron density n_n and the hole density n_p are linked to the quasi Fermi potentials via

$$n_n = N_c \mathcal{F}_n \left(\frac{q(\psi - \varphi_n) - E_c}{k_B T} \right) \quad \text{and} \quad n_p = N_v \mathcal{F}_p \left(\frac{q(\varphi_p - \psi) + E_v}{k_B T} \right), \quad (2.7.4)$$

where N_c and N_v denote the conduction and valence band density of states. The conduction and valence band-edge energies E_c and E_v are defined as material parameters. Since in the literature the definition of band-edge energies is rather heterogeneous, we give an overview in Appendix B.1 of how similar definitions, such as in [9, 10], are related. We assume Fermi-Dirac statistics (2.7.3) for electrons and holes, i.e. $\mathcal{F}_n = \mathcal{F}_p = F_{1/2}$, if not mentioned otherwise.

2.7.2 Ionic vacancies

To model the statistical relationship between densities and potentials (2.6.1) for the ion vacancy densities n_α , $\alpha \in \mathbb{I}_V$, we make the following physically meaningful assumptions:

1. The lower bound for the concentrations of the vacancies can become zero. In this case, all vacancies introduced due to Schottky defects are occupied.
2. There exists a temperature dependent, upper saturation density for the vacancy concentration denoted with $N_\alpha = N_\alpha(T)$. That is, we cannot create arbitrarily many vacancies. For this saturation density, we have $\beta_\alpha N_{SD} \leq N_\alpha \leq \beta_\alpha \bar{n}_L$.

To the best of our knowledge, the second assumption has been neglected in the perovskite literature apart from the simulation tool [21, 22]. So far, the standard statistics (2.6.1) for the ions has been the Boltzmann approximation, see [8, 10, 12, 18]. Such a modelling assumption, however, is unphysical as there is no saturation limit for creating vacancies. We will now derive a statistical relationship between ionic vacancy densities n_α , $\alpha \in \mathbb{I}_V$ and potentials φ_α which respects both assumptions above.

Grand-canonical formalism of ideal lattice gas Let us assume that in a volume Ω_{vol} of perovskite material exist $n_\alpha |\Omega_{vol}|$ vacancies for $\alpha \in \mathbb{I}_V$ which do not interact with other species. The upper bound for the number of the vacancies in the volume Ω_{vol} is thus $N_\alpha |\Omega_{vol}|$ according to our second assumption above. There exist

$$W(n_\alpha, N_\alpha) = \frac{(N_\alpha |\Omega_{vol}|)!}{(n_\alpha |\Omega_{vol}|)! (N_\alpha |\Omega_{vol}| - n_\alpha |\Omega_{vol}|)!}, \quad \alpha \in \mathbb{I}_V, \quad (2.7.5)$$

distinguishable configurations of the vacancies in the volume Ω_{vol} since the vacancies are indistinguishable whereas the Schottky defects are not¹. Every vacancy brings in an energy of $z_\alpha q \psi - z_\alpha E_\alpha$, where the second term corresponds to the energy brought to the system scaled by the elementary charge. The canonical partition function of the system reads

$$Z(n_\alpha, N_\alpha, T, \psi) = W(n_\alpha, N_\alpha) \exp \left(-n_\alpha |\Omega_{vol}| \frac{-z_\alpha E_\alpha + z_\alpha q \psi}{k_B T} \right). \quad (2.7.6)$$

¹The location of the Schottky defects is assumed to be fixed in the lattice. Otherwise one could distribute the vacancies among all possible $\beta_\alpha \bar{n}_L |\Omega_{vol}|$ sites. Such assumption seems to be more realistic, however, it would lead to estimating cumulative binomial distribution instead of using the binomial formula in (2.7.7).

The grand-canonical partition sum reads

$$\begin{aligned} \Xi(z_\alpha q \varphi_\alpha, N_\alpha, T, \psi) &= \sum_{(n_\alpha | \Omega_{vol})=0}^{(N_\alpha | \Omega_{vol})} Z(n_\alpha, N_\alpha, T, \psi) \exp\left(n_\alpha | \Omega_{vol} \left| \frac{z_\alpha q \varphi_\alpha}{k_B T} \right.\right) \\ &= \left[1 + \exp\left(\frac{z_\alpha q \varphi_\alpha + z_\alpha E_\alpha - z_\alpha q \psi}{k_B T}\right) \right]^{N_\alpha | \Omega_{vol}}, \end{aligned} \quad (2.7.7)$$

where $z_\alpha q \varphi_\alpha$ is the electrochemical potential. The grand-canonical potential is then

$$\begin{aligned} J &= -k_B T \log \Xi \\ &= -k_B T N_\alpha | \Omega_{vol} \log \left[1 + \exp\left(\frac{z_\alpha q \varphi_\alpha + z_\alpha E_\alpha - z_\alpha q \psi}{k_B T}\right) \right]. \end{aligned} \quad (2.7.8)$$

The number of the vacancies $n_\alpha | \Omega_{vol}$ in the volume Ω_{vol} is given as a derivative of the grand-canonical potential J with respect to the electrochemical potential of the vacancies $z_\alpha q \varphi_\alpha$, that is,

$$n_\alpha | \Omega_{vol} = -\frac{\partial}{\partial(z_\alpha q \varphi_\alpha)} J = N_\alpha | \Omega_{vol} \frac{\exp\left(\frac{z_\alpha q \varphi_\alpha + E_\alpha - q \psi}{k_B T}\right)}{1 + \exp\left(\frac{z_\alpha q \varphi_\alpha + E_\alpha - q \psi}{k_B T}\right)}. \quad (2.7.9)$$

Thus, the density distribution given by the formula (2.7.9) is equivalent to the Fermi-Dirac integral of order -1 , namely

$$n_\alpha = N_\alpha F_{-1}\left(z_\alpha \frac{q(\varphi_\alpha - \psi) + E_\alpha}{k_B T}\right), \quad \alpha \in \mathbb{I}_v. \quad (2.7.10)$$

From Figure 2.1b, one can clearly see that the ion vacancy density can never become larger than N_α . Similar ideas have been implemented in the drift-diffusion FEM code [22] and have been included in YSZ models [36]. In [37] the relation in (2.7.10) was derived from a phenomenological free energy under the assumption that a vacancy V_α can be occupied by an ionic species β with $\alpha, \beta \in \{A, B, X\}$, where it not necessarily holds that $\alpha \neq \beta$, whereas we assume that $\alpha = \beta$ as stated in Section 2.4. The band-edge energy E_α and the upper bound of the vacancy concentration N_α are model parameters. In analogy to semiconductor theory, we refer to the latter as effective density of states.

2.8 Thermodynamic equilibrium

To avoid unphysical state dissipation [17], thermodynamic consistency is crucial. A model for charge transport is said to be thermodynamically consistent, if it satisfies

$$\mathbf{j}_\alpha = \mathbf{0} \quad \text{implying} \quad \varphi_\alpha = \text{const.}, \quad \text{for all} \quad \alpha \in \{n, p\} \cup \mathbb{I}_v. \quad (2.8.1)$$

Without loss of generality we assume that $\varphi_\alpha = 0$. Due to the gradient structure of the fluxes (2.2.7) thermodynamic consistency of our model follows directly.

2.9 Local electroneutrality

Assuming thermodynamic equilibrium and a vanishing left-hand side in (2.1.1a), at times it may be of interest to compute a locally electroneutral solution ψ_0 . Due to our more general setting we have to

distinguish two cases. For $\mathbf{x} \in \Omega_{\text{intr}}$ we have

$$\begin{aligned} 0 &= n_p(\psi_0, 0) - n_n(\psi_0, 0) - \sum_{\alpha \in \mathbb{I}_v} z_\alpha n_\alpha \\ &= N_v \mathcal{F}_p \left(\frac{E_v - q\psi_0}{k_B T} \right) - N_c \mathcal{F}_n \left(\frac{q\psi_0 - E_c}{k_B T} \right) - \sum_{\alpha \in \mathbb{I}_v} z_\alpha N_\alpha F_{-1} \left(z_\alpha \frac{E_\alpha - q\psi_0}{k_B T} \right) \end{aligned} \quad (2.9.1)$$

and for $\mathbf{x} \in \Omega_{\text{HTL}} \cup \Omega_{\text{ETL}}$

$$0 = N_v \mathcal{F}_p \left(\frac{E_v - q\psi_0}{k_B T} \right) - N_c \mathcal{F}_n \left(\frac{q\psi_0 - E_c}{k_B T} \right) + N_D - N_A, \quad (2.9.2)$$

where the relations (2.7.4) and (2.7.10) are inserted for the vacancy, electron and hole densities. Assuming linear diffusion of the electric current, i.e. modeling the charge carrier statistics with a Boltzmann approximation (2.7.1), the equation (2.9.2) can be solved analytically, yielding

$$\psi_0|_{\Omega_{\text{HTL}} \cup \Omega_{\text{ETL}}} = \frac{E_c + E_v}{2q} - \frac{1}{2} U_T \log \frac{N_c}{N_v} + U_T \operatorname{arcsinh} \left(\frac{N_D - N_A}{2N_{\text{intr}}} \right), \quad (2.9.3)$$

where N_{intr} is the intrinsic carrier density defined by

$$N_{\text{intr}}^2 = N_c N_v \exp \left(-\frac{E_c - E_v}{k_B T} \right). \quad (2.9.4)$$

2.10 Initial and boundary conditions

For $t = 0$, we have to provide initial conditions ψ^0 and φ_α^0 for $\alpha \in \{n, p\} \cup \mathbb{I}_v$ on the whole domain Ω . More precisely, this means

$$\psi(\mathbf{x}, 0) = \psi^0(\mathbf{x}), \quad \text{and} \quad \varphi_\alpha(\mathbf{x}, 0) = \varphi_\alpha^0(\mathbf{x}), \quad \text{for } \mathbf{x} \in \Omega. \quad (2.10.1)$$

2.10.1 External boundary conditions

Ideal ohmic contacts at the metal interfaces are modeled by Dirichlet boundary conditions. On the remaining interfaces one usually imposes homogeneous Neumann boundary conditions. This means, we assume that the external boundary of the spatial domain $\partial\Omega$ is decomposed into $N_O = 2$ ohmic contacts and an artificial interface Γ_N , where we impose Neumann conditions

$$\partial\Omega = \left(\bigcup_{j=1}^{N_O} \Gamma_{D,j} \right) \cup \Gamma_N.$$

For any $j = 1, \dots, N_O$ we set for all $\mathbf{x} \in \Gamma_{D,j}$, $t \in [0, t_F]$

$$\psi(\mathbf{x}, t) = \psi_0(\mathbf{x}) + U_j(t), \quad (2.10.2a)$$

$$\varphi_n(\mathbf{x}, t) = U_j(t), \quad (2.10.2b)$$

$$\varphi_p(\mathbf{x}, t) = U_j(t), \quad (2.10.2c)$$

where U_j corresponds to an applied voltage. The potential ψ_0 can be computed iteratively (or explicitly when assuming a Boltzmann relation), see Section 2.9. Note that by construction of the device

architecture, it holds $\Gamma_{D,j} \subset (\partial\Omega_{\text{HTL}} \cup \partial\Omega_{\text{ETL}}) \setminus \partial\Omega_{\text{intr}}$ and, thus, no boundary conditions for the vacancy quasi Fermi potentials are needed at the ohmic contacts. On the remaining boundaries, we assume homogeneous Neumann boundary conditions for all $\mathbf{x} \in \Gamma_N$, $t \in [0, t_F]$ read as follows

$$\begin{aligned} \nabla\psi(\mathbf{x}, t) \cdot \boldsymbol{\nu} = \mathbf{j}_n(\mathbf{x}, t) \cdot \boldsymbol{\nu} = \mathbf{j}_p(\mathbf{x}, t) \cdot \boldsymbol{\nu} = 0, \quad \text{on } \Gamma_N, \\ \mathbf{j}_\alpha(\mathbf{x}, t) \cdot \boldsymbol{\nu} = 0, \quad \text{on } \partial\Omega_{\text{intr}} \cap \Gamma_N, \quad \alpha \in \mathbb{I}_V, \end{aligned}$$

where $\boldsymbol{\nu}$ is the outer normal vector on the external interface. Other boundary conditions are possible.

2.10.2 Internal boundary conditions

Due to the heterojunctions, we need additional internal boundary conditions on the interfaces between neighboring subdomains. We assume $\partial\Omega_{\text{HTL}} \cap \partial\Omega_{\text{ETL}} = \emptyset$, i.e. we only need additional conditions at the junctions between the intrinsic layer with the transport layers. For this, we define the set $\Sigma_k = \partial\Omega_k \cap \partial\Omega_{\text{intr}}$ of codimension 1 for $k \in \{\text{HTL}, \text{ETL}\}$. This set corresponds to a point in the one-dimensional case, an edge in 2D and a face in 3D. Let $\mathbf{x}_k \in \Sigma_k$. For $f : \Omega \rightarrow \mathbb{R}^d$, $d \in \{1, 2, 3\}$, we define a one-sided limit by

$$f(\mathbf{x}_k; l) := \lim_{\substack{\mathbf{x} \rightarrow \mathbf{x}_k \\ \mathbf{x} \in \Omega_l \\ \mathbf{x}_k \in \Sigma_k}} f(\mathbf{x}).$$

In our case, we have either $\Omega_l = \Omega_{\text{intr}}$ or $\Omega_l = \Omega_k$ for $k \in \{\text{HTL}, \text{ETL}\}$. First, we assume continuity

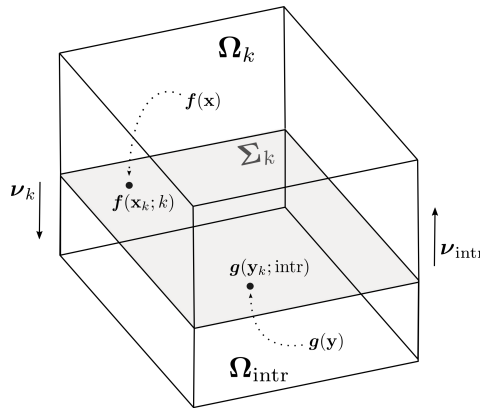


Figure 2.2: Intrinsic domain Ω_{intr} and neighboring domain Ω_k , $k \in \{\text{HTL}, \text{ETL}\}$ with the corresponding notation for interfacial conditions.

on the internal boundaries for the electrostatic potential and the electric displacement [7, 10]:

$$\begin{aligned} \psi(\mathbf{x}_{\text{HTL}}; \text{HTL}) = \psi(\mathbf{x}_{\text{HTL}}; \text{intr}), \quad \varepsilon_s^{\text{HTL}} \nabla\psi(\mathbf{x}_{\text{HTL}}; \text{HTL}) = \varepsilon_s^{\text{intr}} \nabla\psi(\mathbf{x}_{\text{HTL}}; \text{intr}), \\ \psi(\mathbf{x}_{\text{ETL}}; \text{intr}) = \psi(\mathbf{x}_{\text{ETL}}; \text{ETL}), \quad \varepsilon_s^{\text{intr}} \nabla\psi(\mathbf{x}_{\text{ETL}}; \text{intr}) = \varepsilon_s^{\text{ETL}} \nabla\psi(\mathbf{x}_{\text{ETL}}; \text{intr}). \end{aligned}$$

Note that the electric permittivity ε_s is a material dependent parameter. Second, we need conditions for the conservation of the species flux and its associated current density [10], thus we have for $\alpha \in \{n, p\}$

$$\begin{aligned} \mathbf{j}_\alpha(\mathbf{x}_{\text{HTL}}; \text{HTL}) \cdot \boldsymbol{\nu}_{\text{HTL}} = -\mathbf{j}_\alpha(\mathbf{x}_{\text{HTL}}; \text{intr}) \cdot \boldsymbol{\nu}_{\text{intr}}, \\ \mathbf{j}_\alpha(\mathbf{x}_{\text{ETL}}; \text{intr}) \cdot \boldsymbol{\nu}_{\text{intr}} = -\mathbf{j}_\alpha(\mathbf{x}_{\text{ETL}}; \text{ETL}) \cdot \boldsymbol{\nu}_{\text{ETL}}, \end{aligned}$$

where ν_k is the outward unit normal pointing to the set Ω_k , $k \in \{\text{HTL}, \text{ETL}\}$. Third, since ionic species are only present in the intrinsic region, we assume zero flux conditions for the ionic vacancies, i.e. for all $\alpha \in \mathbb{I}_v$ it holds

$$\mathbf{j}_\alpha(\mathbf{x}) \cdot \nu_{\text{intr}} = 0, \quad \text{for } \mathbf{x} \in \Sigma_k, \quad k \in \{\text{HTL}, \text{ETL}\}.$$

Remark 2.10.1. In [10] it is necessary to include additional jump conditions on the charge carrier densities n_n and n_p by multiplying them with specified constants. However, since the quasi Fermi potentials are continuous at the material interfaces our model does not need to take additional internal boundary conditions into account.

2.11 Photogeneration and Recombination

2.11.1 Photogeneration

The photogeneration, i.e. the generation of charge carriers due to the absorption of light, is the most important feature for photovoltaic devices. We can define the generation rate as

$$G(\mathbf{x}) = F_{\text{ph}} \alpha_g \exp(-\alpha_g z), \quad \mathbf{x} = (x, y, z)^T. \quad (2.11.1)$$

Here, F_{ph} denotes the incident photon flux and α_g the material absorption coefficient which depends on the light wave length. We assume that light enters through one of the transport layers. Thus, the photogeneration rate can be described as an exponential decay in z direction, following the Beer-Lambert law of light absorption [38].

2.11.2 Recombination

For the sake of readability, in the following the charge carrier densities of electrons and holes are denoted by $n = n_n$ and $p = n_p$. Within the transport layers and the perovskite, electrons and holes may recombine. The recombination rate $R(n, p)$ on the right-hand side of the charge carrier conservation laws is given by the sum of the most common recombination processes [17]:

$$R(n, p) = \left(r_{\text{rad}}(n, p) + r_{\text{SRH}}(n, p) + r_{\text{Auger}}(n, p) \right) np \left(1 - \exp\left(\frac{q\varphi_n - q\varphi_p}{k_B T}\right) \right),$$

i.e. structurally all these rates can be modeled by the following formula

$$R_r(n, p) = r_r(n, p) np \left(1 - \exp\left(\frac{q\varphi_n - q\varphi_p}{k_B T}\right) \right), \quad (2.11.2)$$

where the model dependent rate r_r will be defined in the following. We note that, the recombination processes stated in the references for the simulation of PSCs [9, 10, 12, 18] assume a Boltzmann relation between the charge carrier densities and the quasi Fermi potentials, yielding an expression

$$\tilde{R}_r(n, p) = r_r(n, p) (np - N_{\text{intr}}^2),$$

where the intrinsic carrier density N_{intr} is defined as in (2.9.4). If using the latter recombination rate and assuming a nonlinear diffusion (2.6.2) consistency with thermodynamic equilibrium in the sense of Section 2.8 is violated.

Radiative recombination The radiative recombination (frequently called *bimolecular* or *band-to-band* recombination) is given by

$$r_{\text{rad}}(n, p) = r_{0, \text{rad}} \quad (2.11.3)$$

for a constant rate coefficient $r_{0, \text{rad}}$.

Shockley-Read-Hall recombination One of the most common recombination processes is the Shockley-Read-Hall (SRH) recombination, which models trapping of electrons. In general, this process can be described by an electron trap continuity equation [39], which implies different recombination rates for electrons and holes. However, a simplified version of this physical process can be given in a closed form when we assume the system to be stationary, namely

$$r_{\text{SRH}}(n, p) = \frac{1}{\tau_p(n + n_\tau) + \tau_n(p + p_\tau)}, \quad (2.11.4)$$

where τ_n, τ_p are the carrier lifetimes and n_τ, p_τ reference carrier densities. These reference densities can be computed with

$$n_\tau = n \exp\left(\frac{E_\tau + q(\varphi_n - \psi)}{k_B T}\right), \quad p_\tau = p \exp\left(\frac{-E_\tau + q(\psi - \varphi_p)}{k_B T}\right),$$

where E_τ denotes the trap energy/level. Choosing the simplified version (2.11.4) is applicable, when assuming that the trapping and detrapping processes are faster than the time scale of measurements [40]. Otherwise this way of defining the SRH recombination needs to be extended as in [12, 18].

Auger recombination For the Auger recombination we have

$$r_{\text{Auger}}(n, p) = C_n n + C_p p$$

with rate constants C_n and C_p . It does not seem to be customary to consider the Auger recombination in perovskites. An exception is given by [41].

2.12 Drift-diffusion model for one mobile ionic species

Since computational experiments [12] show that considering mobile anions as well as mobile cations compared to assuming only mobile anions has relatively little influence, we develop here the special case of only one mobile species, namely the mobile anions X. We denote the corresponding vacancy density by $a = n_{V_X}$ with the corresponding abbreviation in the index, e.g. $E_a = E_{V_X}$. As before, we identify n and p as electron and hole indices with corresponding carrier densities $n = n_n$ and $p = n_p$. In this special case, the Poisson equation in the perovskite is given by (2.5.3), in the transport layers by (2.5.1) and the drift-diffusion model can be formulated as follows: For $\mathbf{x} \in \Omega_{\text{intr}}, t \in [0, t_F]$ we have

$$-\nabla \cdot (\varepsilon_s \nabla \psi) = q(p - n + a - C_0), \quad (2.12.1a)$$

$$\partial_t n - \frac{1}{q} \nabla \cdot \mathbf{j}_n = G(\mathbf{x}) - R(n, p), \quad (2.12.1b)$$

$$\partial_t p + \frac{1}{q} \nabla \cdot \mathbf{j}_p = G(\mathbf{x}) - R(n, p), \quad (2.12.1c)$$

$$\partial_t a + \frac{1}{q} \nabla \cdot \mathbf{j}_a = 0, \quad (2.12.1d)$$

and for $\mathbf{x} \in \Omega_{\text{HTL}} \cup \Omega_{\text{ETL}}$, $t \in [0, t_F]$,

$$-\nabla \cdot (\varepsilon_s \nabla \psi) = q \left((p - N_A) - (n - N_D) \right), \quad (2.12.1e)$$

$$\partial_t n - \frac{1}{q} \nabla \cdot \mathbf{j}_n = G(\mathbf{x}) - R(n, p), \quad (2.12.1f)$$

$$\partial_t p + \frac{1}{q} \nabla \cdot \mathbf{j}_p = G(\mathbf{x}) - R(n, p), \quad (2.12.1g)$$

where the electric currents are defined in (2.2.7).

3 Device simulation

We discretize our model from Section 2.12 via a Scharfetter-Gummel type finite volume method. A short summary of the discretization technique can be found in Appendix A. The parameter set is based on [21, Section 4.4], where the authors compare their drift diffusion solver `Driftfusion` [22] with `Ionmonger` [10].

physical quantity	symbol	value			unit
		ETL	perovskite layer	HTL	
layer thickness		9.9×10^{-6}	4.02×10^{-5}	1.99×10^{-5}	cm
relative permittivity	ε_r	10	24.1	3.0	
conduction band-edge energy	E_c	-4.0	-3.7	-3.1	eV
valence band-edge energy	E_v	-6.0	-5.4	-5.1	eV
conduction band DoS	N_c	5.0×10^{19}	8.1×10^{19}	5.0×10^{19}	cm^{-3}
valence band DoS	N_v	5.0×10^{19}	5.8×10^{19}	5.0×10^{19}	cm^{-3}
electron mobility	μ_n	3.89	66.2	0.389	$\text{cm}^2/(\text{Vs})$
hole mobility	μ_p	3.89	66.2	0.389	$\text{cm}^2/(\text{Vs})$
ion mobility	μ_a	-	3.93×10^{-12}	-	$\text{cm}^2/(\text{Vs})$
density of cation vacancies	C_0	-	1.6×10^{19}	-	cm^{-3}
doping density	N_A	0.0	8.32×10^7	1.03×10^{18}	cm^{-3}
doping density	N_D	1.03×10^{18}	0.0	0.0	cm^{-3}

Table 3.1: Parameter values from [21] for a constant temperature $T = 300\text{K}$.

In the following the importance to correctly model the ion vacancy densities (2.7.10) shall become apparent. To verify our results, we compare them with `Driftfusion` [22]. Just like `Driftfusion` we use the Boltzmann approximation (2.7.1) for the charge carrier densities (2.7.4), i.e. $\mathcal{F}_n = \mathcal{F}_p = \exp$. The model parameter N_a for the mobile anion vacancies is set equal to the uniform density of cation vacancies, i.e. $N_a = C_0 = 1.6 \times 10^{19} \text{cm}^{-3}$. All depicted figures state the physical quantities in an equilibrium state. What we clearly can observe is that limiting the anion vacancy density with the Fermi-Dirac integral of order -1 produces densities and band-edge energies similar to the case without mobile ions. This implies that already in equilibrium the influence of the ions is unphysically overestimated when not limiting the anion vacancy densities as proposed by our modeling approach. Figure 3.1 (e) and (f) reveal that the choice of E_a directly impacts the densities and band-edge energies. For $E_a = -3.9\text{eV}$ we obtain agreement with `Driftfusion` which limits the anion vacancy density with (2.7.10) as well. However, this value differs from $E_a = -4.33\text{eV}$ which was chosen in Figure 3.1 (c) and (d) to produce agreement with `Driftfusion` and `Ionmonger`. Thus, modeling the charge transport with quasi Fermi potentials as suggested in this paper allows to choose the band-edge energy

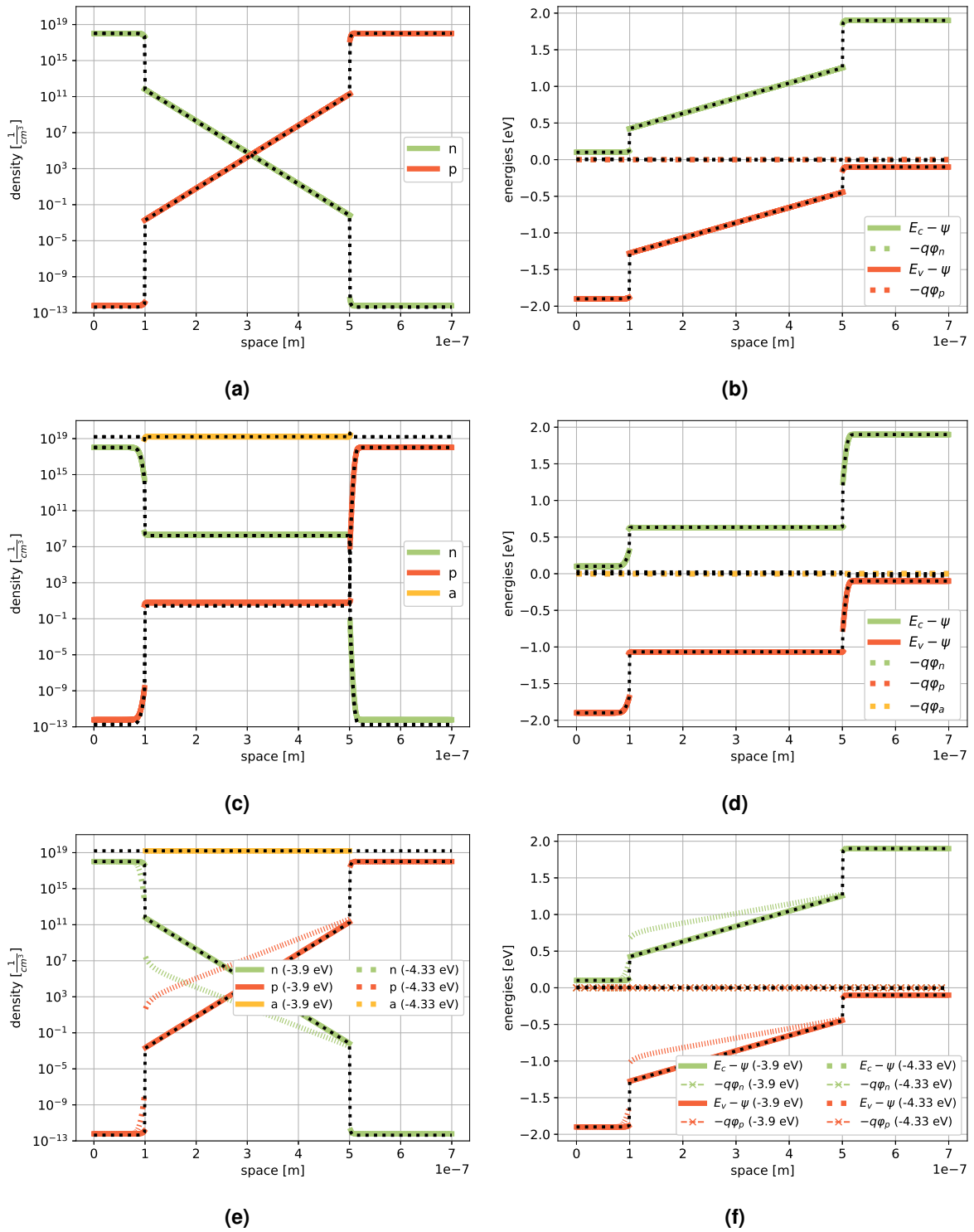


Figure 3.1: Equilibrium charge carrier densities (left) and band-edge energies (right) without mobile ions ((a) and (b)), with mobile ions using Boltzmann statistics ((c) and (d)) and with mobile ions using the Fermi-Dirac integral of order -1 for the anion vacancy density ((e) and (f)). For (c) and (d) we chose $E_a = -4.33\text{eV}$, whereas two different values for E_a were chosen for (e) and (f). Electrons and holes are modeled throughout with Boltzmann statistics. The black dotted lines indicate the corresponding solutions calculated with Driftfusion [22].

in agreement with experiments. Our code is based on `ChargeTransportInSolids` which in turn is based on `VoronoiFVM` [42].

4 Conclusion and future research

We derived a general model for charge transport in perovskite solar cells (PSCs) from Maxwell-Stefan diffusion and electrostatics. In this model any ion in the perovskite layer may be mobile even though one mobile ion seems to be sufficient [12]. Unlike other models in the literature, our model is based on quasi Fermi potentials instead of densities, naturally allowing discontinuities across heterojunctions in the densities. This way we can easily include nonlinear diffusion (via the diffusion enhancement factor based on e.g. Fermi-Dirac, Gauss-Fermi or Blakemore statistics) as well as a limit for ion vacancy depletion (via Fermi-Dirac statistics of order -1). This limit is properly justified by a grand-canonical formalism. From a modeling point of view ion vacancy depletion is physically unrealistic as it would destroy the perovskite structure. For our new model we discussed the thermodynamic equilibrium, electroneutrality as well as generation/recombination mechanisms. Finally, we presented numerical simulations which highlight the importance of limiting ion vacancy depletion. Even in equilibrium the impact of the ions on electrons and holes will be grossly overestimated if one does not limit the ion vacancies. In contrast to the literature on perovskites, we base our simulation on a finite volume method which preserves relevant physical properties such as positivity of densities or constant equilibrium quasi Fermi potentials.

Future research may be directed at including surface recombination for the charge transfer at heterojunctions as already done in [23, 24] as well as coupling our model to another continuity equation for the trap density as has been suggested in [12, 18]. Also more extensive out-of-equilibrium numerical simulations are in preparation.

Acknowledgments This work was partially supported by the German Research Foundation, DFG project no. FU 316/14-1 as well as the Leibniz competition.

A Finite volume discretization

For the one-dimensional spatial discretization of the model (2.12.1), i.e. $\bar{\Omega} = \bar{\Omega}_{\text{ETL}} \cup \bar{\Omega}_{\text{intr}} \cup \bar{\Omega}_{\text{HTL}}$, where $\Omega_{\text{ETL}} =]0, x_E[$, $\Omega_{\text{intr}} =]x_E, x_H[$, and $\Omega_{\text{HTL}} =]x_H, x_F[$, we make use of a thermodynamically consistent Voronoi finite volume technique [17, 32, 43]. For this, we introduce a non-uniform mesh $0 =: x_1 < \dots < x_E < \dots < x_H < \dots < x_n := x_F$. Each node x_k is identified with a control volume ω_k , which is defined as $\omega_1 = [x_1, \frac{x_1+x_2}{2}]$, $\omega_k = [\frac{x_{i-1}+x_i}{2}, \frac{x_i+x_{i+1}}{2}]$, $i = 1, \dots, n-1$, and $\omega_n = [\frac{x_{n-1}+x_n}{2}, x_n]$.

In the following, we pay particular attention to the choice of flux approximations. A correct choice of the numerical fluxes is a rather delicate issue as the wrong choice may lead either to instabilities or violation of thermodynamic principles. For Boltzmann statistics (2.7.1), the classical Scharfetter-Gummel scheme [44] leads to a stable and thermodynamic consistent scheme. Since we consider the system to be potentially non-Boltzmann, we need to handle the nonlinearity in the diffusive part of the current densities j_α , $\alpha \in \{n, p, a\}$. In the literature, Scharfetter-Gummel based flux discretizations which likewise preserve physical properties of the model while still being numerical stable, have recently been developed [17, 27, 45, 46].

We use the following flux approximation. For a node x_k it reads as follows

$$j_{\alpha;k,k+1} = -\frac{q\mu_{\alpha}N_{\alpha}U_T}{z_{\alpha}(x_{k+1} - x_k)} \left(B(-Q_{\alpha;k,k+1})\mathcal{F}_{\alpha}(\eta_{\alpha;k+1}) - B(Q_{\alpha;k,k+1})\mathcal{F}_{\alpha}(\eta_{\alpha;k}) \right),$$

where

$$Q_{\alpha;k,k+1} = z_{\alpha} \frac{\psi_{k+1} - \psi_k}{U_T} + (\eta_{\alpha;k+1} - \eta_{\alpha;k}) - \log \frac{\mathcal{F}_{\alpha}(\eta_{\alpha;k+1})}{\mathcal{F}_{\alpha}(\eta_{\alpha;k})}$$

with

$$\eta_{\alpha;k} = z_{\alpha} \frac{q(\varphi_{\alpha;k} - \psi_k) + E_{\alpha}}{k_B T}.$$

The Bernoulli function is given by $B(\xi) = \xi/(e^{\xi} - 1)$ with $B(0) = 1$. The unknowns ψ_k and $\varphi_{\alpha;k}$ correspond to the electrostatic potential as well as the quasi Fermi potentials for species α evaluated at node x_k . By construction of the mesh, each node x_k corresponds to a set of homogeneous material parameters which makes it possible to handle the heterojunctions in the simulation. The earliest reference, we could find for this thermodynamically consistent flux discretization scheme is in [47]. This scheme was compared in [48] and numerically analyzed in [49].

B Consistency with literature

At first glance, the procedure in Section 2.8 to compute the boundary conditions for the electrostatic potential ψ seems to differ from the approaches known in the literature. Hence, we will show now that they in fact agree. For simplicity, we assume $\Omega = [x_0, x_d] \subset \mathbb{R}$.

B.1 Relating different notations

Comparing e.g. [7, 9, 10, 12], it becomes evident that there are various different terminologies and notations used in the literature. In the following, we focus on the argument of the statistics for electrons and holes, which occurs in (2.7.4) and relate different notations with the one used here. In [9], the quasi Fermi potentials are replaced by the quasi Fermi levels with $q\varphi_n = -E_{F_n}$ and $q\varphi_p = -E_{F_p}$. Due to not necessarily well-defined band-edge energies in the hole and electron transport layers, some references introduce the electron affinity ϕ_{ea} and the ionization potential ϕ_{ip} and replace the band-edge energies in (2.7.4) by these energies, i.e. $E_c = \phi_{ea}$, $E_v = \phi_{ip}$. Furthermore, it is common to define

$$\tilde{E}_c = \phi_{ea} - q\psi, \quad \tilde{E}_v = \phi_{ip} - q\psi,$$

as the band-edge energy, i.e. they include the scaled electrostatic potential ψ [7, 9]. Moreover, [12] considers the lowest unoccupied (LUMO) E_{LUMO} and the highest occupied molecular orbital (HOMO) level E_{HOMO} instead of the energies ϕ_{ea} and ϕ_{ip} . From a physical or chemical point of view we need to distinguish between E_c , E_v on the one hand and E_{LUMO} , E_{HOMO} on the other hand. Since we can assume that E_{LUMO} , E_v , ϕ_{ip} and E_{HOMO} , E_c and ϕ_{ea} play mathematically identical roles, for the sake of readability, we refer to the electron affinity and the ionization potential still as band-edge energies, denoted by E_c and E_v and stick with (2.7.4) even though this is an abuse of terminology.

The built-in voltage is defined as the equilibrium difference between the work functions of the electrodes [7, 10, 12], i.e.

$$\psi_{bi} = \frac{\varphi_{cath} - \varphi_{anod}}{q}, \quad (\text{B.1.1})$$

where φ_{anod} is the anode work function, φ_{cath} is the cathode work function. In case of ideal ohmic contacts (B.1.1) is equal to the difference in equilibrium Fermi levels scaled by the elementary charge. In our terminology this means that the potential ψ_{bi} is the difference of the quasi Fermi potentials at the metal contacts, i.e.

$$\psi_{bi} = \varphi_n(x_d) - \varphi_n(x_0) = \varphi_p(x_d) - \varphi_p(x_0) \stackrel{(2.10.2)}{=} U_2 - U_1.$$

B.2 Boundary conditions

First, we note that relaxing the procedure in Section 2.8 by replacing $\varphi_n = \varphi_p = 0$ with $\varphi_n = \varphi_p = K/2$ for $K \in \mathbb{R}$, yields a modified equation (2.9.2) when assuming a Boltzmann relation (2.7.1), namely

$$0 = N_v \exp\left(\frac{E_v + q(\varphi_p - \hat{\psi}_0)}{k_B T}\right) - N_c \exp\left(\frac{q(\hat{\psi}_0 - \varphi_n) - E_c}{k_B T}\right) + N_D - N_A.$$

When omitting the unphysical solution, this yields

$$\hat{\psi}_0|_{\Omega_{HTL} \cup \Omega_{ETL}} = \frac{1}{2}(\varphi_n + \varphi_p) + \frac{E_c + E_v}{2q} - \frac{1}{2}U_T \log \frac{N_c}{N_v} + U_T \operatorname{arcsinh}\left(\frac{N_D - N_A}{2N_{intr}}\right) \quad (\text{B.2.1})$$

$$= K + \psi_0|_{\Omega_{HTL} \cup \Omega_{ETL}} \quad (\text{B.2.2})$$

with ψ_0 defined by (2.9.3). We see that the conditions in (2.10.2) are shifted by the equilibrium values of the quasi Fermi potentials φ_n and φ_p . Then, the corresponding boundary conditions are

$$\psi(x_0) = K + \psi_0(x_0) + U_1, \quad \psi(x_d) = K + \psi_0(x_d) + U_2, \quad (\text{B.2.3a})$$

$$\varphi_p(x_0) = U_1, \quad \varphi_p(x_d) = U_2, \quad (\text{B.2.3b})$$

$$\varphi_n(x_0) = U_1, \quad \varphi_n(x_d) = U_2. \quad (\text{B.2.3c})$$

In [9], the authors use (ψ, n, p, a) as set of unknowns and impose Dirichlet-Neumann boundary conditions on the external metal contact boundary. In the following, we want to show agreement between (B.2.3) and a modified version of the boundary conditions in [9], namely

$$\begin{aligned} \psi(x_0) &= 0, & \psi(x_d) &= \psi_{bi} - \psi_{ap}, \\ p(x_0) &= p^D, & p(x_d) &= p^{\tilde{D}}, \\ n(x_0) &= n^{\tilde{D}}, & n(x_d) &= n^D, \end{aligned} \quad (\text{B.2.4})$$

where ψ_{ap} denotes the applied voltage and the boundary values are set as

$$n^D = N_c \exp\left(\frac{q\varphi_n(x_d) - E_c}{k_B T}\right), \quad p^D = N_v \exp\left(\frac{E_v - q\varphi_p(x_0)}{k_B T}\right), \quad (\text{B.2.5})$$

$$n^{\tilde{D}} = N_c \exp\left(\frac{q\varphi_n(x_0) - E_c}{k_B T}\right), \quad p^{\tilde{D}} = N_v \exp\left(\frac{E_v - q\varphi_p(x_d)}{k_B T}\right). \quad (\text{B.2.6})$$

To show consistency, we assume the following: (1) $U_1 = 0$, $U_2 = \psi_{ap}$ and (2) $K = -\psi_0(x_0)$. Equations (B.2.5) and (B.2.6) indicate that the conditions for the quasi Fermi potentials (B.2.4) and the conditions for the densities (B.2.3) are equivalent. The conditions for the densities n and p translate directly into conditions for the quasi Fermi potentials. Hence, we focus on the conditions for the electrostatic potential ψ : With Assumptions (1), (2), we see immediately from (B.2.3) that at $x = x_0$, it holds

$$\psi(x_0) = 0. \quad (\text{B.2.7})$$

On the other hand, we have at $x = x_d$

$$-\psi_0(x_0) + \psi_0(x_d) + \psi_{ap} \stackrel{(\text{B.2.3})}{=} \psi(x_d) \stackrel{(\text{B.2.4})}{=} \psi_{bi}(x_d) - \psi_{ap}.$$

Hence, we need to show that

$$\psi_0(x_d) - \psi_0(x_0) + 2\psi_{ap} = \psi_{bi} = \psi(x_d) + \psi_{ap}.$$

By Assumptions (1), (2) and (B.2.7) it follows

$$\begin{aligned} \psi_0(x_d) - \psi_0(x_0) + 2\psi_{ap} &\stackrel{(\text{B.2.3})}{=} (\psi(x_d) - U_2) - (\psi(x_0) - U_1) + 2\psi_{ap} \\ &= \psi(x_d) - \psi(x_0) + \psi_{ap} \stackrel{(\text{B.2.7})}{=} \psi(x_d) + \psi_{ap}. \end{aligned}$$

Hence, the choices of boundary conditions are compatible.

References

- [1] National Renewable Energy Laboratory (NREL), “Best research-cell efficiency chart.” <https://www.nrel.gov/pv/cell-efficiency.html> (accessed 2020-10-09), Jan. 2019.
- [2] N.-G. Park, “Perovskite solar cells: an emerging photovoltaic technology,” *Materials Today*, vol. 18, no. 2, pp. 65 – 72, 2015.
- [3] Helmholtz Zentrum Berlin (HZB), “World record: Efficiency of perovskite silicon tandem solar cell jumps to 29.15 per cent.” https://www.helmholtz-berlin.de/pubbin/news_seite?nid=21020;sprache=en;seitenid=72384 (accessed 2020-10-09), 2020.
- [4] J. Mizusaki, K. Arai, and K. Fueki, “Ionic conduction of the perovskite-type halides,” *Solid State Ionics*, vol. 11, no. 3, pp. 203 – 211, 1983.
- [5] H. J. Snaith, A. Abate, J. M. Ball, G. E. Eperon, T. Leijtens, N. K. Noel, S. D. Stranks, J. T.-W. Wang, K. Wojciechowski, and W. Zhang, “Anomalous hysteresis in perovskite solar cells,” *The Journal of Physical Chemistry Letters*, vol. 5, no. 9, pp. 1511–1515, 2014.
- [6] C. Eames, J. M. Frost, P. R. F. Barnes, B. C. O’Regan, A. Walsh, and M. S. Islam, “Ionic transport in hybrid lead iodide perovskite solar cells,” *Nature Communications*, vol. 6, p. 7497, Nov 2015.
- [7] J. M. Foster, H. J. Snaith, T. Leijtens, and G. Richardson, “A model for the operation of perovskite based hybrid solar cells: Formulation, analysis, and comparison to experiment,” *SIAM Journal on Applied Mathematics*, vol. 74, no. 6, pp. 1935–1966, 2014.
- [8] S. van Reenen, M. Kemerink, and H. J. Snaith, “Modeling anomalous hysteresis in perovskite solar cells,” *The Journal of Physical Chemistry Letters*, vol. 6, no. 19, pp. 3808–3814, 2015.

- [9] P. Calado, A. Telford, D. Bryant, X. Li, J. Nelson, B. O'Regan, and P. Barnes, "Evidence for ion migration in hybrid perovskite solar cells with minimal hysteresis," *Nature Communications*, vol. 7, 2016.
- [10] N. Courtier, J. Cave, A. Walker, G. Richardson, and J. Foster, "Ionmonger: a free and fast planar perovskite solar cell simulator with coupled ion vacancy and charge carrier dynamics," *Journal of Computational Electronics*, vol. 18, pp. 1435–1449, 2019.
- [11] N. E. Courtier, G. Richardson, and J. M. Foster, "A fast and robust numerical scheme for solving models of charge carrier transport and ion vacancy motion in perovskite solar cells," *Applied Mathematical Modelling*, 2018.
- [12] M. T. Neukom, A. Schiller, S. Züfle, E. Knapp, J. Ávila, D. Pérez-del Rey, C. Dreessen, K. P. Zaroni, M. Sessolo, H. J. Bolink, and B. Ruhstaller, "Consistent device simulation model describing perovskite solar cells in steady-state, transient, and frequency domain," *ACS Applied Materials & Interfaces*, vol. 11, no. 26, pp. 23320–23328, 2019.
- [13] D.-H. Doan, A. Glitzky, and M. Liero, "Analysis of a drift–diffusion model for organic semiconductor devices," *Zeitschrift für angewandte Mathematik und Physik*, vol. 70, no. 2, p. 55, 2019.
- [14] A. Glitzky, M. Liero, and G. Nika, "Analysis of a hybrid model for the electrothermal behavior of semiconductor heterostructures," *WIAS Preprint 2636*, 2020.
- [15] A. Mielke, "A gradient structure for reaction–diffusion systems and for energy-drift-diffusion systems," *Nonlinearity*, vol. 24, no. 4, p. 1329, 2011.
- [16] S. M. Sze and K. K. Ng, *Physics of Semiconductor Devices*. Wiley, 2006.
- [17] P. Farrell, D. H. Doan, M. Kantner, J. Fuhrmann, T. Koprucki, and N. Rotundo, "Drift-diffusion models," in *Optoelectronic Device Modeling and Simulation: Fundamentals, Materials, Nanostructures, LEDs, and Amplifiers*, pp. 733–771, CRC Press Taylor & Francis Group, 2017.
- [18] A. Fell, D. Walter, and S. Glunz, "A fast and easy perovskite simulation tool featuring ion migration," in *33rd European Photovoltaic Solar Energy Conference and Exhibition*, 09 2017.
- [19] N. Tessler and Y. Vaynzof, "Insights from device modeling of perovskite solar cells," *ACS Energy Letters*, vol. 5, pp. 1260–1270, 04 2020.
- [20] J. Blakemore, "Approximations for fermi-dirac integrals, especially the function $F_{1/2}(\eta)$ used to describe electron density in a semiconductor," *Solid-State Electronics*, vol. 25, no. 11, pp. 1067 – 1076, 1982.
- [21] P. Calado, I. Gelmetti, B. Hilton, M. Azzouzi, J. Nelson, and P. R. F. Barnes, "Driftfusion: An open source code for simulating ordered semiconductor devices with mixed ionic-electronic conducting materials in one-dimension," 2020.
- [22] I. C. L. Barnes Group, "Driftfusion." <https://github.com/barnesgroupICL>, 2020.
- [23] S. Altazin, C. Kirsch, E. Knapp, A. Stous, and B. Ruhstaller, "Refined drift-diffusion model for the simulation of charge transport across layer interfaces in organic semiconductor devices," *Journal of Applied Physics*, vol. 124, no. 13, p. 135501, 2018.

- [24] Fluxim AG, Switzerland, “Semiconducting thin film optics simulator (SETFOS).” <http://www.fluxim.com>, 2020.
- [25] D. A. Jacobs, H. Shen, F. Pfeffer, J. Peng, T. P. White, F. J. Beck, and K. R. Catchpole, “The two faces of capacitance: New interpretations for electrical impedance measurements of perovskite solar cells and their relation to hysteresis,” *Journal of Applied Physics*, vol. 124, no. 22, 2018.
- [26] J. Xiang, Y. Li, F. Huang, and D. Zhong, “Effect of interfacial recombination, bulk recombination and carrier mobility on the j - v hysteresis behaviors of perovskite solar cells: a drift-diffusion simulation study,” *Phys. Chem. Chem. Phys.*, vol. 21, pp. 17836–17845, 2019.
- [27] P. Farrell, T. Koprucki, and J. Fuhrmann, “Computational and analytical comparison of flux discretizations for the semiconductor device equations beyond Boltzmann statistics,” *J. Comput. Phys.*, vol. 346, pp. 497–513, 2017.
- [28] R. Krishna and J. Wesselingh, “The Maxwell-Stefan approach to mass transfer,” *Chemical Engineering Science*, vol. 52, pp. 861–911, Mar. 1997.
- [29] J. Stefan, “Über das Gleichgewicht und die Bewegung, insbesondere die Diffusion von Gasgemengen,” *Sitzungsberichte der Mathematisch-Naturwissenschaftlichen Classe der Kaiserlichen Akademie der Wissenschaften Wien, 2te Abteilung*, vol. 63, pp. 63 – 124, 1871.
- [30] A. J. Bard and L. R. Faulkner, *Electrochemical Methods: Fundamentals and applications*, vol. 2. Wiley New York, 2001.
- [31] S. van Mensfoort and R. Coehoorn, “Effect of gaussian disorder on the voltage dependence of the current density in sandwich-type devices based on organic semiconductors,” *Physical Review B*, vol. 78, 2008.
- [32] S. Selberherr, *Analysis and Simulation of Semiconductor Devices*. Springer-Verlag, 1984.
- [33] G. Paasch and S. Scheinert, “Charge carrier density of organics with gaussian density of states: Analytical approximation for the gauss-fermi integral,” *Journal of Applied Physics*, vol. 107, 2010.
- [34] J. S. Blakemore, “The parameters of partially degenerate semiconductors,” *Proceedings of the Physical Society. Section A*, vol. 65, pp. 460–461, 1952.
- [35] R. J. Baxter, *Exactly solved models in statistical mechanics*. London, United Kingdom: Academic Press, 1982.
- [36] P. Vágner, C. Gohlke, V. Miloš, R. Müller, and J. Fuhrmann, “A continuum model for yttria-stabilized zirconia incorporating triple phase boundary, lattice structure and immobile oxide ions,” *Journal of Solid State Electrochemistry*, vol. 23, no. 10, pp. 2907–2926, 2019.
- [37] I. Borukhov, D. Andelman, and H. Orland, “Adsorption of large ions from an electrolyte solution: a modified poisson-boltzmann equation,” *Electrochimica Acta*, vol. 46, no. 2, pp. 221 – 229, 2000.
- [38] J. Nelson, *The Physics of Solar Cells*. Series on Properties of Semiconductor Materials, Imperial College Press, 2003.
- [39] T. Goudon, V. Miljanovic, and C. Schmeiser, “On the Shockley-Read-Hall Model: generation-recombination in semiconductors,” *SIAM Journal of Applied Mathematics*, vol. 67, pp. 1183–1201, 01 2007.

- [40] P. Calado, *Transient optoelectronic characterisation and simulation of perovskite solar cells*. PhD thesis, Imperial College London, 2018.
- [41] D. Walter, A. Fell, Y. Wu, T. Duong, C. Barugkin, N. Wu, T. White, and K. Weber, “Transient photovoltage in perovskite solar cells: Interaction of trap-mediated recombination and migration of multiple ionic species,” *The Journal of Physical Chemistry C*, vol. 122, no. 21, pp. 11270–11281, 2018.
- [42] J. Fuhrmann, “VoronoiFVM.jl - Solver for coupled nonlinear partial differential equations based on the Voronoi finite volume method.” <https://github.com/j-fu/VoronoiFVM.jl>, 2019.
- [43] H. Gajewski, “Analysis und Numerik von Ladungstransport in Halbleitern,” *WIAS Report*, vol. 0, no. 6, 1993. ISSN 0942-9077.
- [44] D. Scharfetter and H. Gummel, “Large-signal analysis of a silicon read diode oscillator,” *IEEE Transactions on Electron Devices*, vol. 16, no. 1, pp. 64–77, 1969.
- [45] T. Koprucki, N. Rotundo, P. Farrell, D. H. Doan, and J. Fuhrmann, “On thermodynamic consistency of a Scharfetter-Gummel scheme based on a modified thermal voltage for drift-diffusion equations with diffusion enhancement,” *Optical and Quantum Electronics*, vol. 47, no. 6, pp. 1327–1332, 2015. WIAS preprint 2013.
- [46] M. Patriarca, P. Farrell, J. Fuhrmann, and T. Koprucki, “Highly accurate quadrature-based Scharfetter-Gummel schemes for charge transport in degenerate semiconductors,” *Computer Physics Communications*, vol. 235, pp. 40–49, 2018. WIAS preprint 2498.
- [47] Z. Yu and R. Dutton, “SEDAN III – A one-dimensional device simulator.” www-tcad.stanford.edu/tcad/programs/sedan3.html, 1988.
- [48] M. Kantner, “Generalized scharfetter–gummel schemes for electro-thermal transport in degenerate semiconductors using the kelvin formula for the seebeck coefficient,” *Journal of Computational Physics*, vol. 402, p. 109091, 2020.
- [49] C. Cancès, C. Chainais-Hillairet, J. Fuhrmann, and B. Gaudeul, “A numerical-analysis-focused comparison of several finite volume schemes for a unipolar degenerate drift-diffusion model,” *IMA Journal of Numerical Analysis*, 07 2020.